Characterization of 60 GHz Shadowing by Human Bodies and Simple Phantoms

Gustafson, Carl; Tufvesson, Fredrik

Published in:
6th European Conference on Antennas and Propagation (EUCAP), 2012

DOI:
10.1109/EuCAP.2012.6206265

2012

Characterization of 60 GHz Shadowing by Human Bodies and Simple Phantoms

Carl Gustafson, Fredrik Tufvesson
Department of Electrical and Information Technology, Lund University, Sweden,
email: carl.gustafson@eit.lth.se

***Abstract*—The 60 GHz band is very prominsing for high data rate (>1 Gb/s) wireless systems operating at short ranges. However, due to the short wavelengths in this frequency band, the shadowing effects cuased by human bodies and furniture are severe and needs to be modeled properly. In this paper, we present an experimental, measurement-based characterization of the reflection and shadowing effects in the 60 GHz band caused by human bodies and various phantoms, in order to find simple phantoms suitable for use in human shadowing measurements. It is shown that a water-filled human phantom serves as a good choice for this purpose.**

I. Introduction

Next generation wireless systems operating in the 60 GHz band are currently being designed to provide very high data rates ($>$ 1 Gb/s) for short range communications. Products are already on the market and several standards, such as the *IEEE* standards *802.11ad* [1] and *802.15.3c* [2], are available or under development. Propagation in the 60 GHz band is characterized by a large free-space path loss, low transmission through obstacles and also suffer from sharp shadow zones that can be caused by e.g. furniture or humans. Measurement results have shown that shadowing due to moving human bodies have a significant impact on the propagation of millimeter waves and fading depths of around -20 dB [3] or in the range of -18 to -36 dB [4] have been reported. For propagation and performance analyses, it is therefore of vital importance to have a good model for human interaction such as shadowing and reflection.

Measurements of moving people require real-time systems, which at 60 GHz usually limits the number of Tx and Rx antennas that can be used. Real-time multi-antenna channel sounders at 60 GHz are rare but do exist. Such a channel sounder was presented in [5] and has since been used to characterize the shadowing events due to human bodies using two access points and one Tx [3]. Some measurements do require a larger number of antennas, which can exclude the possibility of using real-time measurements. So far, this has usually been the case when studying the directional properties of the 60 GHz band. Such measurements are typically performed using virtual arrays [6] or highly directional antennas that are mechanically steered [7] and requires that the channel is nearly static. Measurement-based results of the directional properties that also includes the effects of human shadowing are however scarce.

In the literature, ray tracing is often used to simulate the effects of human interaction and the human body is modeled in several different ways. In [8], the authors present a 60 GHz human blockage model developed within the framework of the *IEEE 802.11 Task Group ad*. The model is based on ray tracing and includes a knife edge diffraction model which is an extension of the work in [9]. In [8], the human blockage is modeled using two double knife edges for the body and two single knife edges for diffraction over a human head. In [10], a diffraction based model is used to study network link connectivity, where the human body is approximated by a perfectly conducting cylinder. The authors in [11] employ a ray tracing technique to study human body shadowing at 60 GHz, where the human body is modeled by a cylinder with a partition of salt water that is circumscribed by a parallelepiped. The models used in [8], [10] and [11] are efficient ways to simulate the shadowing effects in the 60 GHz band. However, these effects still needs to be further characterized using measurement based results, and the human body models used in the above studies might not be appropriate for use in measurements.

In more recent studies, 60 GHz human phantoms with appropriate dielectric properties, suitable for use in on-body antenna measurements, are being developed [12], [13]. The aim of this paper is to find a more simple human phantom suitable for use in 60 GHz human shadowing measurements. In such measurements, the Tx and Rx antennas are typically placed at a far-field distance from the shadowing object, and it is only required that the phantom have the appropriate shadowing and reflection properties. For this reason, we present a measurement-based characterization of the shadowing and reflection properties of human bodies and various human phantoms.

II. Measurement Setup and Methods

A. Measurement Equipment and Shadowing Objects

In our measurements, transfer functions were measured using an Agilent E8361A vector network analyzer (VNA). The measured frequency range was 58-62 GHz, using 1601 points, a stepped sweep and an IF-bandwidth of 1 kHz. Fig. 1 shows the basic measurement setup. A V-band horn antenna with a gain of 20 dB was used at both the Tx and Rx. The setup also utilizes a power amplifier (PA) with a gain of 20 dB and a low-noise amplifier (LNA) with a gain of 30 dB, both of which are connected to a high frequency coaxial cable using a coaxial to waveguide transition. High accuracy electromechanical positioners are used to scan the

antennas linearly in a cross section plane of the shadowing object. Since the measurements are performed using a VNA

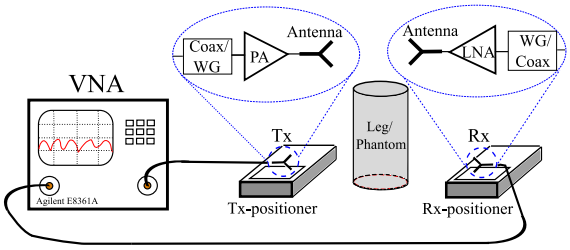

Fig. 1. Measurement setup.

and antenna positioners, it is important that the shadowing object remains still during the entire measurement. Due to the short wavelength of about 5 mm, it is difficult to measure the human blockage since even breathing may cause a person to move too much. For this reason, we initially consider the shadowing due to human legs for the investigation. This makes it easier to make reproducible measurements and to compare the results with simple theoretical models. Four different types of shadowing objects are considered initially: human leg, a plastic cylinder filled with water or wrapped with aluminum foil, and a thin metallic sheet. The cylinder has a diameter of 11 cm and the PVC plastic is about 3 mm thick. The metallic sheet is 11 cm wide and has a thickness of 1 mm. In the measurement of the human legs, the main beam of the antennas were directed at the lower part of one thigh. At this part of the leg, the four different measured legs had approximate diameters in the range of 11-12.7 cm. As a final step, the shadowing of a more realistic human phantom is compared with those of human bodies.

B. Measurement procedure

Two different types of measurements were performed to characterize the shadowing. In the first, one antenna is placed at a fixed and centered position behind the shadowing object. The other antenna is then moved linearly across the width of the object. In the second measurement, both antennas are scanned across the width of the object simultaneously. The distance from each antenna to the object is set to 70 cm, and the polarization is vertical to vertical unless otherwise specified. In each measurement, a line-of-sight (LOS) measurement was performed as a reference, where the shadowing object was removed. The VNA was calibrated and a back-to-back measurement was performed to remove the influence of the coaxial to waveguide transition. The measured data is then post processed to remove the influence of the PA and LNA and then gated in the delay domain to remove contributions from possible multi-path components with delays that are longer than those of the diffracted field. We then define the shadowing gain as

$$g_{\mathrm{S}}(f,\mathbf{r}_{\mathrm{Tx,Rx}}) = H_{\mathrm{Shadow}}(f,\mathbf{r}_{\mathrm{Tx,Rx}})/H_{\mathrm{LOS}}(f,\mathbf{r}_{\mathrm{Tx,Rx}}),$$

where H_{Shadow} and H_{LOS} are the post processed frequency transfer functions of the shadowing and LOS measurements, respectively, and $\mathbf{r}_{\mathrm{Tx,Rx}}$ denotes the position of the Tx/Rx.

C. Diffraction by a Perfectly Conducting Cylinder

The diffraction around a perfectly conducting cylinder, as shown in Fig. 2, can be analytically calculated using a model based on the geometrical theory of diffraction (GTD) [14]. A normally incident wave with a linearly polarized E-field in the z-direction is assumed. The amplitude of the incident E-field

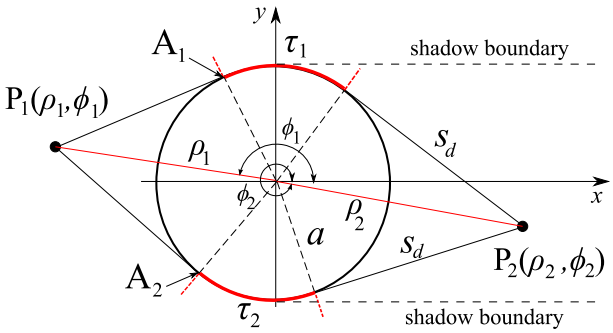

Fig. 2. Diffraction around a perfectly conducting cylinder.

reaching the glancing points A_1 and A_2 is denoted E_i. The diffracted E-field at the position P_2, E_z, can then be written as

$$E_z = \sum_{n=1}^{N} D_n^e E_i \frac{\exp(-jks_d)}{\sqrt{8jks_d}} \times \Big[\exp\{-(jk+\Omega_n^e)\tau_1\} + \exp\{-(jk+\Omega_n^e)\tau_2\}\Big]$$

The incident rays each travel a distance along the cylinder (τ_1 and τ_2) and are attenuated according to the attenuation constant Ω_n. For the E-field, this constant is given by

$$\Omega_n^e = \frac{\alpha_n}{a} M \mathrm{e}^{j\pi/6}. \tag{1}$$

Finally, D_n and M are each given by

$$D_n = 2M\{\mathrm{Ai}'(-\alpha_n)\}^{-2}\mathrm{e}^{j\pi/6}, \quad M = \left(\frac{ka}{2}\right)^{1/3} \tag{2}$$

Here, $-\alpha_n$ denotes the zeros of the Airy function $\mathrm{Ai}(\cdot)$, k is the wavenumber and a is the radius of the cylinder.

D. Dielectric Properties

The dielectric proerties of human tissue is of importance when developing human phantoms. At 60 GHz, the penetration depths in tissues are typically small, which could indicate that it is important that the outer layer of the phantom has dielectric properties similar to those of human skin. Table 1 lists some typical values of the complex permittivity, $\epsilon_c = \epsilon' - j\epsilon''$, at 60 GHz, for human skin, fat, muscle and of pure water at 20° C. We note that the dielectric properties of pure water at 20°

C are more or less similar to those of muscles. For a more detailed discussion about the dielectric properties at 60 GHz, the reader is referred to [12] and the references therein.

TABLE I
COMPLEX PERMITTIVITY AT 60 GHZ

	ϵ_c	Ref.
Skin	$7.98 - j10.91$	[15]
Fat	$2.51 - j0.84$	[15]
Infiltrated Fat	$4.40 - j3.13$	[15]
Muscle	$12.85 - j15.74$	[15]
Water (20° C)	$11.9 - j19.5$	[12]

The dielectric properties of PVC plastics at 70 GHz and above have been reported to have typical values around $\epsilon_{c,\mathrm{PVC}} = 2.9 - j0.03$ [16], which indicates that the dielectric loss in PVC at 60 GHz is low compared to skin. However, this also indicates that the real part of the permittivity of PVC at 60 GHz could be similar to that of uninfiltrated fat. A PVC phantom could be covered with an appropriate layer with dielectric properties similar to those of skin to create a layered model of the human skin/fat layers. This is however outside the scope of this paper.

III. RESULTS

A. Theoretical and Measured Shadowing Gain

Fig. 3 shows the measured and theoretical shadowing gain for the metallic cylinder when the Tx and Rx are moved simultaneously across the width of the cylinder. The theoretical curve was calculated using the GTD model described above. The curves show a good overall agreement with a slightly worse agreement close to the edge of the shadowing boundary. This can be attributed to the fact that the theoretical GTD model used is no longer valid close to the transition region about the shadow boundary. However, in the deep shadow region, the GTD model can predict the shadowing gain accurately and shows that the diffracted field can be described by so called *creeping waves* along the surface of the cylinder.

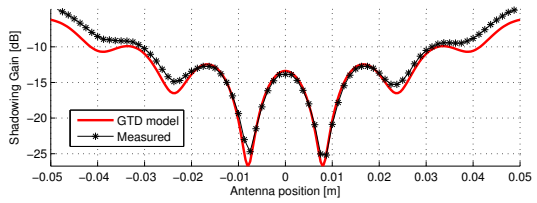

Fig. 3. Shadowing gain for the metallic cylinder and for the GTD model. The Tx and Rx are moved simultaneously across the width of the cylinder.

Using the GTD model, the shadowing gain was calculated for different metallic cylinders with radii ranging from 5-25 cm. The result is shown in Fig. 4. As a reference, the radius of the cylinder used to model the human body in [11] is 15 cm.

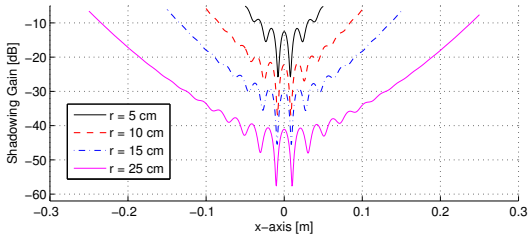

Fig. 4. Calculated shadowing gain for metallic cylinders with different radii, using the GTD model.

B. Shadowing Gain for various Shadowing Objects

Fig. 5(a) shows the measured shadowing gain for different shadowing objects as a function of Tx position with the Rx at a fixed position. All objects show similar diffraction patterns with slightly different shapes. The diffraction patterns for the legs display assymetry, which could be explained by the fact that the legs are not perfectly cylindrical. The metallic and water filled cylinder show a better agreement to the shadowing gain of the legs as compared to the metallic sheet.

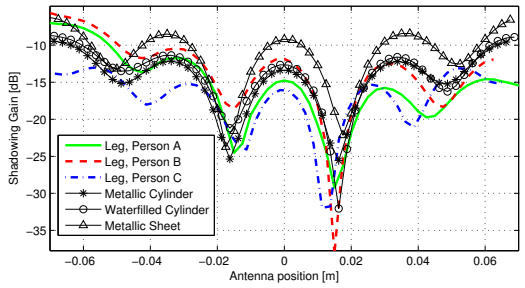

(a)

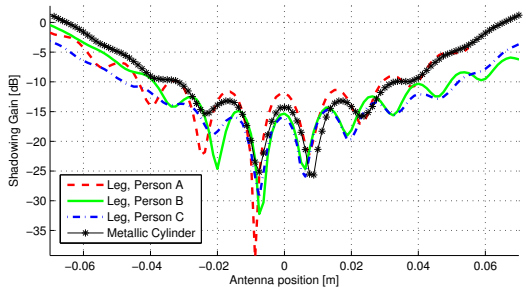

(b)

Fig. 5. Shadowing gain for different shadowing objects with (a) a fixed Rx and (b) with the Tx and Rx moved simultaneously.

In Fig. 5(b), both the Tx and the Rx are moved simultaneously, which makes the diffraction dips occur more frequently over distance. Again, the metallic cylinder shows a good agreement with the shadowing gain of the legs, especially for person A. The leg of this person had a diameter of approxiamtely 11.3 cm, which is close to the diameter of the cylinder.

C. Polarization

So far, only vertical-to-vertical polarization has been considered. For this reason, the shadowing gain of a persons leg was measured using both vertical-to-vertical (V-V) and horizontal-to-horizontal (H-H) polarization. The result is seen in Fig. 6, which shows that the shadowing loss is greater for V-V polarization. This is due to a higher diffraction loss for fields that are parallel to the surface of the shadowing object. For this particular measurement, the difference between V-V and H-H polarization is about 5-6 dB in the deep shadow region. However, this difference could be even greater for other shadowing objects where the waves traverse a longer distance along the surface of the shadowing object. When considering a more general shadowing scenario, it is difficult to say if V-V or H-H polarization is to be preferred, since diffraction may occur around the shoulder, head or the sides of a person.

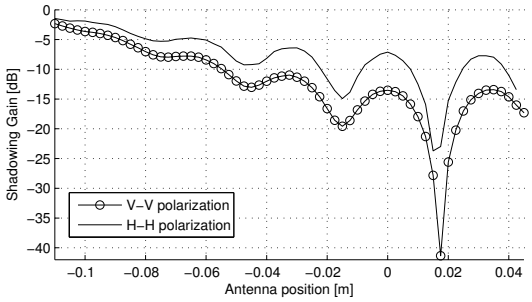

Fig. 6. Shadowing Gain for a leg, with vertical-to-vertical and horizontal-to-horizontal polarization.

D. Reflection

The diffraction patterns of the metallic and water filled cylinder turned out to be quite similar. However, in order to find an appropriate phantom suitable for use in measurements, the reflection needs to be considered as well. Fig. 7 shows the measured reflection for the metallic cylinder, the waterfilled cylinder and a human leg. The reflection from the metallic cylinder is more than 4 dB higher than for the waterfilled cylinder, while the reflection from the leg is fairly similar to that of the waterfilled cylinder.

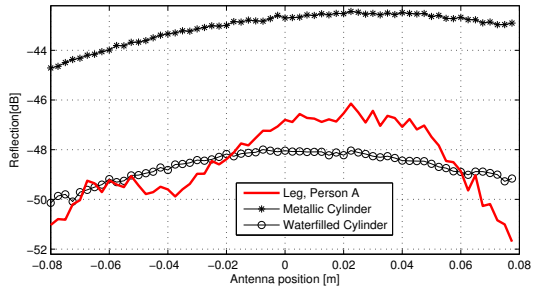

Fig. 7. Measured reflection from a human leg and the metallic and waterfilled cylinders.

E. A Realistic Human Phantom

For reasons explained above, only simple phantoms have been considered so far. The next step is to try to find a human phantom with a more realistic shape, that also is suitable for use in measurements. Since the water-filled PVC cylinder had reflection and shadowing properties similar to those of a human leg, it could be reasonable that a water-filled human phantom would be a good candidate for 60 GHz shadowing measurements. In order to verify if this is the case, a series of measurements were performed, comparing the shadowing gain of the water-filled human phantom shown in Fig. 8 with those of three different persons. The shell of this phantom is made of a type of fiberglass and has a thickness of about 3 mm, which is the same as for the PVC cylinder. The dielectric properties of this shell at 60 GHz is however unknown, which is an issue. The dashed line in Fig. 8 indicates the distance over which the

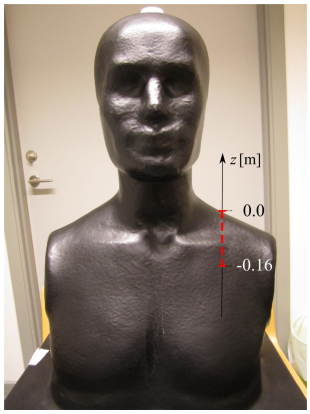

Fig. 8. A human phantom. The dashed line indicates the distance over which the antennas are scanned.

antennas were scanned, resembling a scenario where a person stands up and blocks the line-of-sight between the Tx and Rx Again, both antennas were scanned simultaneously over this distance and the polarization is V-V. Then, the phantom was replaced with humans and great care was taken to ensure that the persons were sitting as close as possible to the original position of the phantom. Each person tried to remain as still as possible during the duration of the entire measurement. The measured shadowing gain for the three persons and the human phantom is seen Fig. 9. The shadowing gain of all three persons show higher values in the deeper shadow region when compared to the human phantom. The curve for person A shows a trend similar to the human phantom, which could indicate that the human phantom is suitable for use in measurements. Additional measurements are currently being performed in order to more effectively determine if this phantom have the desired reflection and shadowing properties. This particular phantom does not have any arms, which could influence the results. Also, a larger set of measurements is needed to assess the influence of varying body sizes as well as to characterize the typical shadowing features of an average

person. Finally, the influence of clothing might need to be investigated as well, since few examples of this exist at 60 GHz [17].

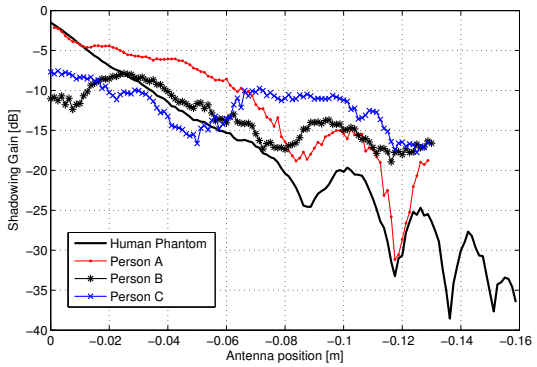

Fig. 9. Shadowing gain for the human phantom and three different persons.

IV. Conclusions

We have performed a measurement based investigation of the 60 GHz shadowing gain of human bodies and various phantoms in order to find a phantom suitable for use in measurements. It has been concluded that the measured shadowing gain of human legs are similar to those of the phantoms that were studied. The best agreement was found for the metallic and water-filled cylinder. The metallic sheet also showed a similar pattern with a slighlty higher gain. However, from a measurement point of view, any knife edge type of phantom, such as the metallic sheet, has the drawback of being sensitive to the exact orientation of the phantom. Furthermore, the reflection properties of such a phantom would be an issue. Comparing the reflection properties of a human leg with those of the metallic cylinder, it was found that the reflection from the metallic cylinder was higher than for the leg by around 4 dB. The water-filled cylinder on the other hand, showed a fairly good agreement with the reflection from the human leg. Based on these results, a water-filled human phantom with a more realistic shape was then considered. This phantom was found to have similar shadowing properties similar to those of humans but with a slightly higher loss. This shows that the water filled human phantom is most likely appropriate for use in 60 GHz human shadowing measurements.

References

[1] Status of Project IEEE 802.11ad - Very High Throughput in 60 GHz, URL: http://www.ieee802.org/11/Reports/tgad_update.htm

[2] S-K. Yong, et al.,TG3c channel modeling sub-commitee final report, *IEEE Techn. Rep.*,15-07-0584-01-003c, 2007.

[3] A. P. Garcia, W. Kotterman, R. S. Thoma, U. Trautwein, D. Brckner, J. Kunisch, "60 GHz Time-Variant Shadowing Characterization within an Airbus 340", COST2100, Wien, Austria, Sep. 2009.

[4] S. Collonge, G. Zaharia and G. E. Zein, "Influence of the Human Activity on Wideband Characteristics of the 60 GHz Indoor Radio Channel", *IEEE Transactions on Wireless Communications* 3(6), 2389-2406.

[5] A. P. Garcia, W. Kotterman, R. S. Thoma, U. Trautwein, D. Brckner, W. Wirnitzer, J. Kunisch, "60 GHz in-Cabin Real-Time Channel Sounding", 3rd Int. Workshop on Broadband MIMO Channel Measurement and Modeling - IWonCMM, Xi'an, China, August 25, 2009.

[6] C. Gustafson, F. Tufvesson, S. Wyne, K. Haneda and A. F. Molisch, "Directional Analysis of Measured 60 GHz Indoor Radio Channels using SAGE", *IEEE 73rd Vehicular Technology Conference* (VTC Spring), 2011.

[7] H. Xu, V. Kukshya and T. S. Rappaport, "Spatial and Temporal Characteristics of 60-GHz indoor Channels", *IEEE Journal on Selected Areas in Communications*, Vol. 20, No. 3, April 2002.

[8] M. Jacob, S. Priebe, A. Maltsev, et al., "A ray tracing based stochastic human blockage model for the IEEE 802.11ad 60 GHz channel model," *Antennas and Propagation (EUCAP)*, 11-15 April 2011.

[9] J. Kunisch and J. Pamp, "Ultra-wideband double vertical knife-edge model for obstruction of a ray by a person", *IEEE ICUWB*, 2008.

[10] S. Singh, et al., "Blockage and Directivity in 60 GHz Wireless Personal Area Networks: From Cross-Layer Model to Multihop MAC Design" *IEEE Journal on Selected Areas In Communications*, 2009.

[11] A. Khafaji, R. Saadane, J. El Abbadi and M. Belkasmi, "Ray Tracing Technique based 60 GHz Band Propagation Modelling and Influence of People Shadowing" *World Academy of Science, Engineering and Technology*, 2008.

[12] N. Chahat, M. Zhadobov, R. Sauleau and S. I. Alekseev, "New Method for Determining Dielectric Properties of Skin and Phantoms at Millimeter Waves Based on Heating Kinetics", *IEEE Tans. on Microwave Theory and techniques*, January 2012.

[13] N. Chahat, M. Zhadobov, S. Alekseev and R. Sauleau, "Human skin-equivalent phantom for on-body antenna measurements in the 60 GHz band," *Electron. Lett.*, to appear.

[14] G. L. James, "Geometrical Theory of Diffraction for Electromagnetic Diffraction", 3rd ed., *IEEE Electromagnetic Wave Series*.

[15] S. Gabriel, R. W. Lau and C. Gabriel, "The dielectric properties of biological tissues: III. Parametric models for the dielectric spectrum of tissues", *Phys. Med. Biol.* 41 (1996) 22712293.

[16] A.Elhawil, L. Zhang , J. Stiens, C. Tandt, N. A. Gotzen, G. V. Assche and R. Vounckx, "A Quasi-Optical Free-Space Method for Dielectric Constant Characterization of Polymer Materials in mm-wave Band", Proceedings Symposium IEEE/LEOS Benelux Chapter, 2007, Brussels.

[17] , M. Zhadobov, N. Chahat, R. Sauleau, C. L. Quement and Y. L. Drean, "Millimeter-wave interactions with the human body: state of knowledge and recent advances", *International Journal of Microwave and Wireless Technologies*, 2011, 3(2), 237247.